EROSIVE BURNING OF COMPOSITE PROPELLANTS*

Merrill K. King

Atlantic Research Corporation
Alexandria, Virginia 22314

ABSTRACT

Increasing use of solid rocket motors with low port-to-throat area ratios, including the ultimate case of nozzleless motors, is leading to increased occurrence and severity of burning rate augmentation due to flow of propellant products across burning propellant surfaces (erosive burning). A review of the literature regarding this phenomenon indicates a lack of systematic data defining the effects of propellant formulation variables on the sensitivity of burning rate to crossflow velocity and the absence of a realistic predictive model for composite propellant burning rate-pressure-velocity relationships. In this paper, a physically realistic picture of the effect of crossflow velocity on composite propellant combustion is presented and a relatively simple analytical model based upon this picture is developed for prediction of composite propellant burning rate as a function of pressure and crossflow velocity, given only the burning rate-pressure relationship in the absence of crossflow. In addition, hardware developed for testing erosive burning effects at cross flow Mach Numbers up to 1.0 is described and a planned systematic test matrix is defined. Preliminary test results are included and compared with predictions made using the aforementioned analytical model.

INTRODUCTION

Development of a better understanding of the effects of crossflows on solid propellant combustion is needed for accomplishment of accurate motor performance predictions in terms of both mean interior ballistics analysis and prediction of motor stability characteristics. With such understanding, the motor designer can either design his grains to compensate for mean erosive burning effects on grain burn pattern, or, knowing how propellant formulation parameters affect erosion sensitivity, vary propellant parameters in such a way as to minimize these effects.

In recent years, requirements for ever higher propellant mass fractions in solid propellant rocket motors and for higher thrust-to-weight ratios have led to development of centrally perforated grain configurations with relatively low port-to-throat area ratios. This, in turn, results in high velocities of propellant gases across burning propellant surfaces in the aft portions of these grains, leading to erosive burning. Moreover, a series of studies has demonstrated that the nozzleless rocket concept offers significant economic advantages over a more conventional rocket system when considered for some tactical weapon systems. This concept requires that the flow within the bore or central perforation of a grain accelerate to the point that sonic conditions are achieved at the aft end. In this situation, the high velocity environment results in

*This study is supported by AFOSR under Contract No. F44620-76-C-0023, monitored by Major Thomas Meier.

(19) 1251

EROSIVE BURNING OF COMPOSITE PROPELLANTS

(9) INTERIM rept.

6. PERFORMING ORG. REPORT NUMBER

7. AUTHOR(s)

(10) MERRILL K. KING

8. CONTRACT OR GRANT NUMBER(s)

(15) F44620-76-C-0023

9. PERFORMING ORGANIZATION NAME AND ADDRESS

ATLANTIC RESEARCH CORPORATION
5390 CHEROKEE AVENUE
ALEXANDRIA, VA 22314

10. PROGRAM ELEMENT, PROJECT, TASK AREA & WORK UNIT NUMBERS

61102F (16) 2308A1 (17) A1

11. CONTROLLING OFFICE NAME AND ADDRESS

AIR FORCE OFFICE OF SCIENTIFIC RESEARCH/NA
BLDG 410
BOLLING AIR FORCE BASE, D C 20332

12. REPORT DATE

(11) Nov 76

13. NUMBER OF PAGES

29 (12) 31 p.

14. MONITORING AGENCY NAME & ADDRESS (if different from Controlling Office)

15. SECURITY CLASS. (of this report)

UNCLASSIFIED

15a. DECLASSIFICATION/DOWNGRADING SCHEDULE

16. DISTRIBUTION STATEMENT (of this Report)

Approved for public release; distribution unlimited.

17. DISTRIBUTION STATEMENT (of the abstract entered in Block 20, if different from Report)

18. SUPPLEMENTARY NOTES

19. KEY WORDS (Continue on reverse side if necessary and identify by block number)

EROSIVE BURNING
COMPOSITE PROPELLANTS
SOLID ROCKET MOTORS
NOZZLELESS MOTORS

20. ABSTRACT (Continue on reverse side if necessary and identify by block number)

Increasing use of solid rocket motors with low port-to-throat area ratios, including the ultimate case of nozzleless motors, is leading to increased occurrence and severity of burning rate augmentation due to flow of propellant products across burning propellant surfaces (erosive burning). A review of the literature regarding this phenomenon indicates a lack of systematic data defining the effects of propellants formulation variables on the sensitivity of burning rate to crossflow velocity and the absence of a realistic predictive model for composite propellant burning rate-pressure-velocity relationships. In this

DD FORM 1 JAN 73 1473 EDITION OF 1 NOV 65 IS OBSOLETE

UNCLASSIFIED 045 550

SECURITY CLASSIFICATION OF THIS PAGE (When Data Entered)

paper, a physically realistic picture of the effect of crossflow velocity on composite propellant combustion is presented and a relatively simple analytical model based upon this picture is developed for prediction of composite propellant burning rate as a function of pressure and crossflow velocity, given only the burning rate-pressure relationship in the absence of cross-flow. In addition, hardware developed for testing erosive burning effects at cross flow Mach numbers up to 1.0 is described and a planned systematic test matrix is defined. Preliminary test results are included and compared with predictions made using the aforementioned analytical model.

substantial erosive burning, with burning rates significantly higher than those measured in a conventional strand bomb being encountered.

Nozzleless rockets present a unique challenge to analytical understanding because the gas velocity reaches sonic and supersonic velocities on the grain surfaces, leading to a realm of erosive burning never before considered. The effects are critical in that the erosive burn rate contributions strongly influence performance level, performance repeatability and thrust misalignment. More than in any conventional motor, the exact erosive burn rate behavior must be held constant from batch to batch if reproducibility is not to be a problem. The performance sensitivity of a nozzleless motor to erosion is due to the fact that the maximum erosion occurs at the choke point in the base. Since this point is the effective throat area, and the throat area versus time is thus a function of regression rate, the result is a chamber pressure history which varies strongly with erosion.

Erosive burning can have a very dominant influence on rocket performance. Consider, for example, a motor with a centrally perforated grain whose erosive burning characteristics may be approximated empirically by:

$$\varepsilon = r/r_o = 1 + k_2 M \tag{1}$$

where:

ε = erosion ratio
r = burning rate in presence of crossflow at Mach Number M
r_o = burning rate at same pressure with no crossflow
k_2 = empirical constant
M = crossflow Mach Number.

In this case, the fractional increase in burning rate due to erosion at the aft end of the motor is given by:

$$\frac{r_{aft} - r_{fore}}{r_{fore}} = k_2 M_{aft} \tag{2}$$

A typical value of the erosion constant k_2 is of the order of unity. Hence, the burning rate at the aft-end is very sensitive to the gas flow. For a grain with an initial port-to-throat ratio of 1.6, for a propellant specific heat ratio of 1.25, the Mach Number through the port will vary from 0 at the head end to 0.5 at the aft end, tending to increase the aft end burning rate to 50 percent greater than that at the fore end. This erosive effect will, of course, be partially compensated for by decreased static pressure at the aft end associated with the high velocity flow and with total pressure losses due to channel flow with mass addition. The static pressure change along a centrally perforated grain is given approximately by:

$$\frac{P_{fore}}{P_{aft}} = 1 + \gamma M^2_{aft} \tag{3}$$

where γ is the heat capacity ratio of the propellant gases (taken to be 1.25 in this example). The fractional burning rate decrease due to pressure drop at the aft-end is obtained by substituting equation (3) into a non-erosive burning rate expression, resulting in:

$$\frac{r_{fore} - r_{aft}}{r_{fore}} = 1 - (1 + \gamma M_{aft}^2)^{-n} \qquad (4)$$

where n is the pressure exponent of the burning rate. For a value of n of approximately 0.5, the change in burning rate due to pressure decrease can be neglected up to at least $M_{aft} = 0.3$. Even at $M_{aft} = 0.5$ the fractional decrease is only 12%, compared to an increase at the aft-end of 50 percent due to erosive effects. Thus, shortly after ignition, the propellant will be regressing approximately 35% faster at the aft end than at the fore end, a factor which will have to be allowed for by the motor designer in trying to arrive at a desired thrust-time behavior.

Since there is such a strong interaction between the local flow environment and the propellant burning rate, it is necessary to be able to predict this interaction in order to design and calculate the performance of a low port/throat area ratio rocket (particularly a nozzleless rocket with a port/throat area ratio of unity). A review of the literature has indicated that there is no unifying model or theory which can be used to reliably predict the propellant burning rates in an erosive situation.

General observations of importance from past experimental studies (1-10) include:

1. Plots of burning rate versus gas velocity or mass flux at constant pressure are usually not fitted best by a straight line.
2. Threshold velocities and "negative" erosion rates are often observed.
3. Slower burning propellants are more strongly affected by crossflows than higher burning-rate formulations.
4. At high pressure, the burning rate under erosive conditions tends to approach the same value for all propellants (at the same flow velocity) regardless of the burning rate of the propellants at zero crossflow.
5. Erosive burning rates do not depend upon gas temperature of the crossflow (determined from tests in which various "driver propellants" products are flowed across a given test propellant).

There is, however, very little data available for high crossflow velocities (greater than $M \gtrsim 0.3$). In addition, there has been no study in which various propellant parameters have been systematically varied one at a time. Such a study is necessary for determination of erosive burning mechanisms and proper modeling of the erosive burning phenomena. Much of the past work has not resulted in instantaneous (as opposed to averaged over a range of pressure and crossflow velocity) measurements of erosive burning rates under well characterized local flow conditions.

From the above discussion, it is apparent that development of an analytical model of erosive burning, properly describing the physical effects which result in augmentation of solid composite propellant burning rate by crossflows, coupled with an experimental effort to systematically define the effects of various formulation parameters on erosive burning at crossflow velocities up to Mach 1 is of great importance to the design and development of advanced solid rocket systems.

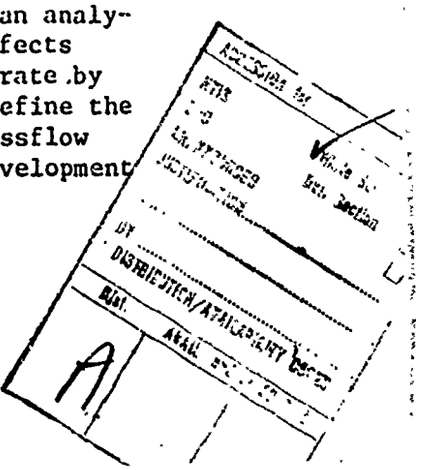

ANALYTICAL MODELING

Brief Review of Past Modeling Efforts

The objectives of a theoretical model of erosive burning are to provide a means of predicting the sensitivity of propellant combustion rate to gas flow parallel to the ablating surface and to indicate what effect various formulation parameters have on this sensitivity. An acceptable model must account for: (1) any effects observed when crossflow gas temperature is varied; (2) observed pressure dependency; and (3) nullification of catalyst activity under erosive conditions. This model should provide an explanation of the observed behavior in terms of the hydrodynamic conditions induced by a crossflow coupled with the chemical and physical processes that constitute the propellant deflagration mechanism.

As part of this study, a large number of models of erosive burning phenomena have been reviewed. The authors of the more significant of these are listed in Table I. As indicated in that table, these models generally fall into one of three categories. The first is based upon the assumption that the erosive burning is driven by increased heat transfer from the mainstream gas flow associated with increased heat transfer coefficient with increased mass flux parallel to the grain surface. The best-known and most widely used model, that of Lenoir and Robillard (11), falls into this category. (See Table II for a Summary Review.) In this model, the authors state that the total burning rate (r) is the sum of two effects: a rate dependent on pressure (r_p, earlier referred to as r_o, the normal burning rate), and a second erosive rate (r_e) dependent upon the combustion gas flow rate. This equation entails an assumption that the pressure-dependent "base" rate, r_o, is unaffected by an increase in total rate at a given pressure, an assumption which almost certainly cannot be true. This problem has been discussed in detail by King (21), with derivation of a modified Lenoir and Robillard expression allowing for the coupling of flame standoff distance with burning rate. While Lenoir and Robillard assume $r = r_o + r_e$, allowance for this coupling results in $r = (r_o^2/r) + r_e$. In physical terms, Lenoir and Robillard have failed to account for the fact that increased burning rate, caused by erosive feedback at constant pressure, results in the propellant flame being pushed further from the surface, decreasing its heat feedback rate, and thus decreasing the propellant burning rate part of the way back toward the base rate.

The weaknesses of the Lenoir and Robillard theory are that it provides no physical picture of the erosion process in terms of interactions of the hydrodynamics with chemical and physical processes involved in the propellant deflagration, it contains two free constants which must be obtained by best-fitting data for each propellant, the additivity of the non-erosive and erosive burning rate components is handled incorrectly as discussed above, and the theory predicts substantial dependence on the temperature of the core gas [which dependence was found to be completely absent by Marklund and Lake (7)]. Analysis of the Lenoir and Robillard treatment indicates that the erosive contribution to burning rate, r_e is given by:

$$r_e \propto G^{0.8} \mu_{gas}^{0.2} (T_{core\ gas} - T_{surface}) \qquad (5)$$

(where G is the mass flux of the crossflow) for a given test propellant and

given geometry. But at fixed crossflow velocity and pressure, G is inversely proportional to the core gas (driver propellant products) temperature while μ_{gas} is roughly directly proportional to this temperature. Therefore,

$$r_e \alpha T_{core\ gas}^{-0.6}(T_{core,gas} - T_s). \tag{6}$$

However, Marklund and Lake performed a set of experiments in which crossflow velocity and pressure were held constant while the driver propellant was changed from a 1700°K propellant to a 2500°K propellant, with T_s being approximately 800°K in both cases. Thus, the Lenoir and Robillard theory would indicate that:

$$\frac{r_{e,\ 2500°K\ driver}}{r_{e'\ 1700°K\ driver}} = \frac{1700}{900}\left(\frac{2500}{1700}\right)^{-0.6} = 1.50 \tag{7}$$

That is, with the higher driver gas temperature case, the erosive burning rate component of the total burning rate should be 50 percent higher than that for the low driver gas temperature. However, as mentioned, Marklund and Lake observed no difference in erosive rates in the two cases. This observed lack of dependence of the erosive burning rate on core gas temperature tends to put all the models in the first category in Table I on shaky grounds.

The model of Zucrow, Osborn, and Murphy (12) is worthy of particular attention, since it is the only model known to this writer which permits prediction of negative erosion which has been observed in some cases. However, it may be shown that this prediction results from a physically impossible result of a mathematical extrapolation. The basic burning rate expression employed is:

$$r = r_o + \frac{h(T_{Combustion} - T_{surface,\ Avg.})}{Q\rho_{prop}} \tag{8}$$

where Q is basically the heat required to preheat and vaporize unit mass of the propellant (with some corrective adjustments) and h is the heat transfer coefficient from the core gas to the propellant surface. Ancillary expressions used include:

$$h = h_o(C_h/C_{ho}) \tag{9}$$

$$C_h/C_{ho} = 1 - \beta_T B \tag{10}$$

$$B = \rho_{prop} r_o / C_{ho} G \tag{11}$$

where β_T is a constant transpiration parameter and C_{ho} and h_o are the Stanton Number and the heat transfer coefficient in the absence of crossflow, all other parameters being as defined earlier.

The difficulty lies in the use of Equation 10 for the ratio of the Stanton Number with crossflow to that without crossflow. This expression should only be used for values of $B_T B << 1$. As it is, at sufficiently small values of G, B exceeds $1/\beta_T$. When this occurs, Equation 10 yields a negative value for the Stanton Number (violating the Second Law of Thermodynamics) and thus the heat transfer coefficient h becomes negative and the second term

of Equation 8 also becomes negative, yielding a predicted burning rate, r, less than the burning rate in the absence of cross-flow, r_o. The correct limit for C_h/C_{ho} as $G \to 0$ ($B \to \infty$) is unity, while Equation 10 predicts it to go to minus infinity.

The models of Saderholm (2) and Marklund (7) are not vastly different from that of Lenoir and Robillard, except that Saderholm totally ignores the "base" (no crossflow) burning rate in comparison to the erosive contribution, a treatment that seems a bit drastic, particularly for fairly low crossflow velocities.

The second category of models listed in Table I includes models based upon the alteration of transport properties in the region between the gas flame and the propellant surface by the crossflow, generally due to turbulence effects. Included in this category are models in which the thermal conductivity in this region is raised by turbulence and models in which the time for consumption of fuel gas pockets leaving the surface is reduced by the effects of turbulence on diffusivity. Four of these models were developed for double-base propellants as indicated, and will not be reviewed here.

The models of Lengelle (17) and Saderholm, Biddle, Caveny, and Summerfield (18) for composite propellant erosive burning are somewhat similar in principle, though the latter model is applied to the special case of very-fuel-rich propellants at quite low crossflows. The basic propellant combustion mechanism assumed is the granular diffusion model in which pockets of fuel vapor leave the surface and burn away in an oxidizer continuum at a rate strongly dependent upon the rate of micromixing of the oxidizer vapor into the fuel vapor pocket. The driving mechanism by which the crossflow is assumed to increase the burning rate is through increased turbulence associated with increasing crossflow raising the turbulent diffusivity in the mixing region (thus increasing the rate of mixing and decreasing the effective distance of the diffusion flame from the surface) and raising the effective turbulent thermal conductivity. Both the decrease in distance from heat release zone to surface and the increase in thermal conductivity increase the heat flux to the surface, thus causing the propellant to ablate more quickly. There are several notable weaknesses associated with the Lengelle model: (1) the granular diffusion flame model is not physically realistic; (2) the ammonium perchlorate monopropellant flame is ignored; and (3) the boundary layer treatment used to calculate the dependence of the effective turbulent diffusivity and conductivity on the crossflow is unrealistic in its use of a 1/7th power velocity law all the way from the free-stream to the surface.

In the third category of model listed in Table I, models based upon chemically reacting boundary layer theory, we have found only one model, that of Tsuji for a homogeneous propellant. It is appreciated that, as pointed out by Williams, Barrere and Huang (22), a full-blown aerothermochemical modeling approach to erosive burning with full coupling of aerodynamic boundary layer and combustion processes is an extremely difficult undertaking. Unfortunately, the Tsuji attempt is not very useful due to the assumption of a totally laminar boundary layer and limitation to a situation where the free-stream velocity is proportional to the distance from the head-end of the grain. Other simplifications include assumption of premixed stoichiometric fuel and oxidizer (rendering the model inapplicable to

composite propellant systems) and use of one-step global kinetics.

Current Model Development

The proper approach to the theoretical modeling of the erosive burning process of composite propellants is to specify a physical-chemical mechanism for the normal burning of such propellants, to analyze the boundary layer conditions for the type of mass flow that is occurring in rocket motors, and then to couple the two processes.

Considering first the flow process, let us estimate what the flow profiles and angles look like near the surface of a propellant for a typical erosive burning situation. As an example, let us choose a case where the operating pressure is 6,890,000 N/m^2 (1000 psi), the propellant flame temperature is 2500°C, the crossflow mainstream velocity is 91.5 m/sec (300 ft/sec), the characteristic length dimension for determining Reynold's Number is 15 cm (0.5 feet), and the propellant burning rate is 1.25 cm/sec (0.5 in/sec). In this case, the gas velocity away from the surface at the flame temperature is approximately 3m/sec (10 ft/sec). Using flow profile data in the presence of transpiration from Mickley and Davis (23), we estimate that the crossflow velocity 10μ from the propellant surface is about 6 m/sec (20ft/sec), at 20μ from the surface about 9 m/sec (30 ft/sec) and at 40μ from the surface, about 12 m/sec (40 ft/sec). An "effective flame standoff distance" of about 20μ can be calculated for a burning rate of 1.25 cm/sec (0.5 in/sec). This simply represents an effective distance from the surface (based upon energy balance considerations) where the heat would have to be released to cause the grain to ablate at this rate. (Note that this is a greatly simplified picture just to demonstrate scales of events.) Thus we arrive at the very rough picture shown in Figure 1. The important thing to note is the resultant flow paths shown as the heavy dashed lines in this figure. (Actually, they may well be curved rather than straight, since, while velocity away from the surface increases with the increasing temperature away from the surface and velocity parallel to the surface also increases with distance from the surface, the two components of the vector do not necessarily have the same dependence upon distance from the surface. That is, their ratio is not necessarily independent of distance from the surface.)

The important feature of this picture is that any diffusion flame at the AP-binder boundaries is bent over toward the propellant surface by the crossflow velocity. Since the deflection of this mixing column or cone can be shown to cause the distance from the base to the tip, measured perpendicular to the base, to decrease, the height above the propellant at which any given fraction of the mixing of AP products and fuel decomposition products is complete should, therefore, be decreased and the distance from the propellant surface to the "average" location of the diffusion flame should also be decreased. This, in turn, will increase heat feedback and thus increase burning rate. The schematic of a composite propellant erosive burning model based upon this picture is shown in Figure 2.

In the first part of the figure, we picture the flame processes occurring in the absence of crossflow. There are two flames considered, an ammonium perchlorate deflagration monopropellant flame close to the surface and a columnar diffusion flame resulting from mixing and combustion of the AP deflagration products and fuel binder pyrolysis products at an average

distance somewhat further from the surface. Three important distance parameters considered are the distance from the propellant surface to the "average" location of the kinetically controlled AP monopropellant heat release (L_I), the distance associated with mixing of the oxidizer and fuel for the diffusion flame (L_{Diff}), and the distance associated with the fuel-oxidizer reaction time subsequent to mixing (L_{Kin}). A heat balance between heat feedback from these two flames and the energy requirements for heating the propellant from its initial temperature to the burning surface temperature and decomposing it yields (assuming that the heat feedback required per unit mass of propellant consumed is independent of burning rate):

$$r\alpha\dot{q}_{feedback} \propto \frac{k_1(T_{AP\ flame} - T_s)}{L_I} + \frac{k_2(T_{flame} - T_s)}{L_{Diff} + L_{Kin}} \qquad (12)$$

The situation pictured as prevailing with a crossflow is shown in the second part of Figure 2. Since L_I and L_{Kin} are both kinetically controlled and are thus simply proportional to a characteristic reaction time (which is assumed to be unaffected by the crossflow) multiplied by the propellant gas velocity normal to the surface (which for a given formulation is fixed by burning rate and pressure alone) these distances are fixed for a given formulation at a given burning rate and pressure, independent of the crossflow velocity. Of course, since crossflow velocity affects burning rate at a given pressure through its influence on the diffusion process as discussed below, L_I and L_{Kin} are influenced through the change in burning rate, but this is simply coupled into a model by expressing L_I and L_{Kin} as explicit functions of burning rate and pressure in that model. The important point is that they can be expressed as functions of these two parameters alone for a given propellant. However, the distance of the mixing zone from the propellant surface is directly affected by the crossflow. It may be shown through geometrical arguments coupled with the columnar diffusion flame height analysis presented by Schultz, Penner and Green (4), that L_{Diff} measured along a vector coincident with the resultant crossflow and transpiration velocities should be approximately the same as L_{Diff} in the absence of a crossflow at the same burning rate and pressure (except at very high ratios of local crossflow velocity to transpiration velocity). That is, the magnitude of L_{Diff} is essentially independent of the crossflow velocity, although its orientation is not. Thus, the distance from the surface to the "average" mixed region is decreased to $L_{Diff} \sin\theta$ where θ represents the angle of the average flow vector in the mixing region. The heat balance at the propellant surface now yields:

$$r \propto \dot{q}_{feedback} \propto \frac{k_1(T_{AP,flame} - T_s)}{L_I} + \frac{k_2(T_{flame} - T_s)}{L_{Diff}\sin\theta + L_{Kin}} \qquad (13)$$

During the past year, a model based upon this picture for prediction of burning-rate versus pressure curves at various crossflow velocities from a no-crossflow burning rate versus pressure curve has been developed. This model employs no empirical constants other than those backed out of analysis of the no-crossflow burning rate data. Thus, although it is not as powerful as a model which would permit prediction of erosive burning phenomena with no burning rate data at all, but only propellant composition and ingredient

size data, it is still a very useful tool in that it permits prediction of erosive burning characteristics given only relatively easily obtained strand-bomb burning rate data. (By comparison, the Lenoir and Robillard model employs two free constants which are adjusted to provide a best fit of erosive burning data for a given propellant and since these constants vary from propellant to propellant, the Lenoir and Robillard model does not permit a priori erosive burning predictions for new propellants without some erosive burning data, whereas the model presented here does not require such data.)

The general approach followed in development of this model was:

1. Derive expressions for L_I, L_{Diff}, and L_{Kin} as functions of burning rate (or burning mass flux, $\dot{m}_{burn}$), pressure, and propellant properties and substitute these into a propellant surface heat balance.

2. Work the resulting equation into the form (developed in succeeding paragraphs):

$$r = A_3 P \left[1 + \frac{A_4}{1 + A_5 d_p^2 P^2}\right]^{1/2}$$

for burning in the absence of crossflow and perform a regression analysis using no-crossflow burning rate data to obtain best fit values for A_3, A_4, and A_5. (d_p is the average ammonium perchlorate particle size. For a given propellant, the burning rate data may be just as effectively regressed on A_3, A_4, and $A_5 d_p^2$, eliminating the necessity of actually defining an effective average particle size.)

3. From these results, obtain expressions for L_I, L_{Diff}, and L_{Kin} as functions of burning rate (or $\dot{m}_{burn}$) and pressure.

4. Combine these expressions with an analysis of the boundary layer flow (which gives the crossflow velocity as a function of distance from the propellant surface, mainstream velocity, and propellant burning rate) to permit calculation of the angle θ (Figure 2), L_I, L_{Diff}, L_{Kin}, and $\dot{m}_{burn}$ for a given pressure and crossflow velocity.

In the derivation of a burning rate expression for a composite propellant in the absence of a crossflow, an energy balance at the propellant surface is first written as: (See Figure 2.)

$$\frac{\lambda_A (T_f - T_s)}{(L_{Diff}) + (L_{Kin})} + \frac{\lambda_B (T_{AP} - T_s)}{L_I} = \dot{m}[C_p (T_s - T_{AMB}) + Q_{VAP} - Q_{RX}] \quad (14)$$

where:

λ_A, λ_B = thermal conductivity, with an area ratio term for each flame lumped in.
T_f = final flame temperature.
T_s = surface temperature.
T_{AP} = ammonium perchlorate monopropellant flame temperature.

L_{Diff}, L_{kin}, L_I = as shown in Figure 2.
$\dot{m}$ = mass propellant burning flux (linear burning rate x propellant density).
C_p = average propellant heat capacity.
T_{AMB} = unburned propellant bulk temperature.
Q_{VAP} = heat per unit mass involved in various endothermic processes at or below the propellant surface, e.g., binder pyrolysis or AP sublimation.
Q_{RX} = heat per unit mass involved in various exothermic processes at or below the propellant surface.

The first term of this equation represents heat flux from the final flame to the surface, the second represents heat flux from the AP monopropellant flame, and the third represents the heat flux requirements for ablation of the propellant at the mass flux, $\dot{m}$. Several simplifying assumptions are obviously involved in writing of the equation in this form. Probably the most important and tenuous of these is the assumption that Q_{RX} is independent of burning rate (or $\dot{m}$) and of pressure. In the Zeldovich picture of solid propellant combustion, where subsurface exothermic reactions with fairly high activation energies are considered to dominate, this would be a very poor assumption, but in the generally accepted picture of solid propellant combustion in this country, it is not a bad approximation. In addition, it is assumed that the surface temperature is nearly constant with respect to pressure and burning rate, with the resultant uncoupling of this heat balance equation from a surface regression rate Arrenhius expression. Finally, it is assumed that for the diffusion flame, a distance associated with mixing may be added linearly to a distance associated with reaction delay to yield a total flame offset distance, a fairly gross simplification.

The monopropellant AP flame offset distance, L_I, may be expressed as the product of a characteristic reaction time, τ_I, and the linear velocity of gases leaving the propellant surface:

$$L_I = \tau_I \frac{\dot{m}}{\rho_{gas}} \tag{15}$$

For a second-order gas-phase reaction (generally assumed), τ_I is inversely proportional to pressure, and for a given formulation, the gas density is directly proportional to pressure, yielding:

$$L_I = K_1 \dot{m}/P^2 \tag{16}$$

A similar analysis for L_{Kin} yields:

$$L_{Kin} = K_2 \dot{m}/P^2 \tag{17}$$

For a columnar diffusion flame, it may easily be shown (24) that the diffusion cone height, L_{Diff}, may be expressed as:

$$L_{Diff} = K_3 \dot{m} d_p^2 \tag{18}$$

where d_p is the ammonium perchlorate particle size.

Equations 14 and 16 through 18 may be combined with much manipulation to yield:

$$\dot{r} = \dot{m}/\rho_{propellant} = A_3 P \left[1 + \frac{A_4}{1 + A_5 d_p^2 P^2} \right]^{1/2} \tag{19}$$

Burning rate versus pressure data for a given propellant in the absence of a crossflow may then by analyzed via a fairly complicated regression analysis procedure to yield values of the constants A_3, A_4, and A_5 (or $A_5 d_p^2$) for that given propellant. The constants K_1, K_2, and K_3 are related to these constants in turn by:

$$K_1 = \frac{(T_{AP} - T_s)\lambda_B}{A_2 A_3^2 \lambda_A} \tag{20}$$

$$K_2 = \frac{(T_f - T_s)}{A_2 A_3^2 A_4} \tag{21}$$

$$K_3 = \frac{(T_f - T_s) A_5}{A_2 A_3^2 A_4} \tag{22}$$

where:

$$A_2 = \frac{\rho_{prop}^2 [C_p (T_s - T_{bulk}) + Q_{VAP} - Q_{RX}]}{\lambda_A} \tag{23}$$

In this analysis a rough estimate of A_2 has been made to permit calculation of values of K_1, K_2, and K_3 from the best-fit values of A_3, A_4, and A_5. It should be pointed out, however, that the subsequent calculations of burning rates in crossflows are virtually unaffected by the estimate of A2, since the same value of A_2 is used in that analysis, and thus its effects essentially wash out. The value used for most cases (except those cases run to test the effect of A_2) was $2 \cdot 10^6$ gm sec °K/cm^5.

Data of Mickley and Davis (23) were used to develop empirical expressions for the local crossflow velocity as a function of distance from the propellant surface, mainstream crossflow velocity, and transpiration rate (gas velocity normal to the propellant surface). In this analysis, it was decided that the transpiration velocity ($V_{Transpiration}$) should be calculated as the gas velocity normal to the surface at the final flame temperature since the mainstream velocity used was also that at the final flame temperature. (Mickley and Davis correlations are based upon the ratio of mainstream velocity to transpiration velocity.) The procedure used is outlined in Table III.

The above analyses were used in the derivation of the following eight equations in eight unknowns for the burning of a given composite propellant at a given pressure and crossflow velocity:

$$\dot{r} = \frac{K_2'}{L_{Diff} \sin\theta + L_{Kin}} + \frac{K_7'}{L_I} \tag{24}$$

$$L_{Diff} = K_1' \dot{r} \tag{25}$$

$$L_{Kin} = K_5' \dot{r} \tag{26}$$

$$L_I = K_6' \dot{r} \tag{27}$$

$$V_{transpiration} = K_3' \dot{r} \tag{28}$$

$$Y^+_{y=L_{Diff}\sin\theta} = K_8' \dot{r} \sin\theta$$

$$U_{Crossflow,\ y=L_{Diff}\sin\theta} = K_9' f\left(Y^+_{y=L_{Diff}\sin\theta}\right) \tag{30}$$

$$\text{Sin}\ \theta = V_{transpiration} \Big/ \sqrt{V^2_{Transpiration} + U^2_{Crossflow,y=L_{Diff}\sin\theta}} \tag{31}$$

where:

$$K_1' = \frac{(T_f - T_s) A_5\, d_p^2\, \rho_{prop}}{A_2 A_3^2 A_4} \tag{32}$$

$$K_2' = \rho_{prop} (T_f - T_s)/A_2 \tag{33}$$

$$K_3' = \frac{R\, T_f\, \rho_{prop}}{P\ (MW)} \tag{34}$$

$$K_5' = \frac{(T_f - T_s)\rho_{prop}}{A_2 A_3^2 A_4\, P_2} \tag{35}$$

$$K_6' = \frac{(T_{AP} - T_s)\ \rho_{prop}\ \lambda_B}{A_2 A_3^2\, P^2\, \lambda_A} \tag{36}$$

$$K_7' = [\rho_{prop}(T_{AP} - T_s)/A_2]\ (\lambda_B/\lambda_A) \tag{37}$$

$$K_8' = \frac{K_1'\, U^*\, \rho_{gas,\ T = (T_f + T_s)/2}}{\mu_{gas,\ T = (T_f + T_s)/2}} \quad \text{(See Table III)} \tag{38}$$

$$K_9' = U^* \quad \text{(See Table III)} \tag{39}$$

and the function f of Equation 30 is given in Table III.

Implicit in Equation 31 is the assumption that the transpiration

velocity and the crossflow velocity maintain a constant ratio from very near the surface out to the end of the diffusion zone; that is, that the vector resultant is a straight line as sketched in Figure 1. This approximation is probably not seriously in error, and should not strongly affect the results of the calculations.

As may be seen, the quantity A_2 appears in the denominator of K_2', K_7', K_1', K_5', and K_6'. Thus, as indicated earlier, the effect of A_2 washes out of Equation 24 and the predicted burning rate is dependent upon this parameter only to the extent that it affects the calculation of the crossflow velocity at distance $L_{Diff} \sin \theta$ from the surface. Parametric calculations with various values of A_2 indicate that this effect is very weak.

A computer code has been developed to solve these equations simultaneously, yielding a predicted burning rate for a given pressure, crossflow velocity and set of constants A_3, A_4, and $A_5 d_p^2$ obtained from regression analysis of no-crossflow data. Thus far, only one set of systematic erosive burning rate data has been located which has sufficient zero crossflow burning rate data to permit calculation of these constants, a set of data taken by Saderholm (2). The code has been used to calculate burning rate versus pressure curves for several crossflow velocities studied by Saderholm, with and without the corrections of the boundary layer profiles for transpiration effects. The results are shown in Figures 3 and 4. As may be seen, without correction for the effects of transpiration on the boundary layer profile, burning rates are badly overpredicted (Figure 3), not unexpectedly. However, with the transpiration correction factor included, the agreement between experiment and prediction is excellent, as shown in Figure 4.

EXPERIMENTAL

Equipment Design

Previous investigators of erosive burning have generally utilized one of two experimental approaches. One approach involves interrupted-burning studies of grains tailored to insure erosive burning, measuring the changes in bore diameter which have occurred up to the point of quenching, and trying to relate these changes to some model which will predict the observed pressure-time curve (normally a total pressure measured at the forward end of the grain where local flow velocities are low). The second approach consists of placing a small peice of propellant in a high velocity blast tube and determining its burn time through the changes in the overall pressure time curves. The first approach suffers from a problem of averaging (average burn rates being obtained over a period during which pressure and/or velocity vary around average values), while the latter approach suffers in general from hydrodynamics being considerably different than those obtained in motors. The work to date has, in general, not resulted in instantaneous measurements of erosive burning rates under well-characterized local flow conditions. This, coupled with a lack of data in the high Mach Number region ($M \geq 0.5$) and a lack of studies in which propellant parameters are systematically varied one at a time under identical hydrodyanamic conditions has resulted in an incomplete understanding of erosive burning phenomena.

In the present program, we will measure erosive burning rates at high pressures over a wide range of crossflow Mach Numbers. It is difficult to

achieve these conditions of pressure and velocity and measure them simultaneously with instantaneous burning rates. The chosen test apparatus is depicted in Figure 5. A driver grain which is used to produce the high velocity gas flow across the test grain is a 6C4 grain (15.2 cm outside diameter, 10.2 cm inside diameter cylindrically perforated grain), burning on the inside surface only, whose length is chosen to yield the required operating pressure level for any given test. Standard double-length 6C4 hardware is used for this part of the test apparatus. Bolted to the end of the 6C4 motor tube is a contoured transition section, approximately 10 cm (4 inches) long, which channels the gases from the driver grain into the rectangular test section. The test grain extends from the test section back through the transition section to butt against the driver grain to eliminate leading edge effects which would be associated with a test grain standing alone. The test grain is approximately 30 cm (12 inches) long (plus the 10 cm extending through the transition section) by 1.90 x 2.50 cm (3/4 inch x 1 inch) web and burns only on the 1.90 cm face. The flow channel of the test section is initially 1.90 cm x 1.90 cm (3/4 inch x 3/4 inch) opening up to 1.90 cm x 4.45 cm (3/4 inch x 1-3/4 inch) as the test propellant burns back through its 2.54 cm (1 inch) web. For higher Mach Number tests, the apparatus is operated in a nozzleless mode with the gases choking at or near the end of the test grain, while for lower Mach Number tests, a 2-dimensional nozzle is installed at the end of the test channel. All sizes were chosen after preliminary parametric interior ballistics design. The 2.54 cm web was chosen since it is a convenient match to existing 6C4 hardware and, moreover, yields a total test time of 1 to 10 seconds for propellant burning rates of 0.25 to 2.5 cm/sec, a range of interest. The 1.90 by 1.90 cm initial test channel size was chosen as the largest possible size consistent with reasonable driver grain lengths and weights required for operation at the highest operating pressure and crossflow velocity desired for the test matrix with the chosen formulations.

During each test, pressure and crossflow velocity varies with time and location along the test grain. (For the nozzleless tests, pressure varies significantly with time and location, while crossflow velocity varies considerably with location but not significantly with time. For tests using a nozzle with an initial port to throat area ratio of 1.5 or higher, on the other hand, pressure does not vary strongly with location, but does rise with time due to the progressivity of the driver grain, while crossflow velocity varies strongly with time and slightly with location.) These variations permit design of tests to yield considerable burning rate-pressure-crossflow velocity data in relatively few tests, provided that these parameters can be measured continuously at several locations along the test grain. These parameters are measured in the following manner.

The burning rate is directly measured by photographing the ablating grain with a high-speed motion picture camera through a series of four glass windows located along the length of the test section. (See Figures 5 and 6.) Frame by frame analysis of the films permits determination of instantaneous burning rate as a function of time at each of the four window locations. The windows are flush mounted on the inside of one side wall and sealed with "O"-ring seals. Further details of the window design are given below.

For nozzled cases, the measured location of the burning propellant surface at each window as a function of time, together with the known

constant throat area, permits straightforward calculation of the crossflow velocity as a function of time. However, the very sensitive dependence of Mach Number on area ratio for M > 0.5 makes calculation of crossflow velocity from area ratio measurement quite poor for nozzleless cases. Accordingly, for these tests, stagnation pressure is measured at the aft end of the test section and used in combination with the measured driver chamber pressure for calculation of the stagnation pressure in the test section as a function of time and position. (Static pressure wall taps at each window location are used for measurement of static pressure as a function of time for both nozzled and nozzleless cases.) From the static and stagnation pressure values determined as a function of time and position down the test section, crossflow Mach Number and velocity are calculated as a function of time at each window location in the test section for the nozzleless cases.

Detailed thermal and stress analyses have been carried out for design of the hardware to handle:

(1) Propellant flame temperature up to 3500°K.
(2) Operating pressure up to 1500 psia.
(3) Driver grain length up to 22 inches.
(4) Mass flow rates up to 10 pounds/second.
(5) Mach Number in test section up to 1.0.
(6) Burn time up to 10 seconds.
(7) Mass of propellant up to 20 pounds.

These values have been calculated to permit operation over the range of propellant compositions, pressures, and crossflow velocities desired.

As indicated earlier, standard heavywall 6C4 hardware already on hand is being used for the driver grains. The transition section is an insulated water-cooled steel piece which bolts to the aft end of the 6C4 hardware as an aft closure. The test section in turn is bolted to the transition section. A detailed drawing of the test section, emphasizing the viewing window layout is shown in Figure 6. This figure is largely self-explanatory. The flow gap is surrounded by propellant on one side and asbestos phenolic on the other three sides, with circular cutouts in the asbestos phenolic through which the inner part of the windows butt flush against the propellant. (Inner and outer window sections are used, since it is anticipated that at least under the more severe test condtions the inner window surface will suffer damage during the test or during post-test cooldown.) Detailed analysis of the expected thermal response of the windows has been performed. This analysis indicates that quartz windows should be quite satisfactory for all early tests, which employ relatively low flame temperature (less than 2400°K) propellants. As testing progresses to higher flame temperature propellants substitution of a special high-temperature clear RTV potting compound for the inner quartz window may be required. To date, tests with low flame temperature formulations with either quartz or RTV inner windows have been satisfactory, as long as the side of the test propellant is adequately inhibited to prevent any side-burning, and quite satisfactory films have been obtained.

Test Matrix - Selection Rationale

Six "scholastic" formulations have been identified for initial study.

(These are referred to as "scholastic" formulations in that they are formulations specifically chosen to permit systematic variation of well-defined composition and ingredient-size parameters, including the use of unimodal ammonium perchlorate particle size, but as a consequence are not formulations being currently considered for mission applications.) It is considered that the use of unimodal oxidizer in early testing is important since any model permitting prediction of burning rate-pressure-crossflow velocity characteristics from first principles will almost certainly be first derived for unimodal oxidizer. (Methods of handling multimodal oxidizer sizes for predictions of burning rate, even in the absence of crossflows, are still the subject of considerable debate.) In addition, it appears foolish to face the added experimental and modeling problems associated with metal additives early in the program. Accordingly, these initial formulations will be nonmetalized. The use of unimodal oxidizer, however, is the chief factor rendering the initial formulations "scholastic," since such a restriction drastically limits the maximum solids loading, and accordingly results in relatively low flame temperature propellants. (Of course, this is also beneficial as regards initial testing, since it permits checkout of the hardware under less severe conditions with extension to more severe conditions being held in abeyance until considerable practical experience in operation of the equipment has been developed.)

The six "scholastic" formulations chosen for initial study are listed in Table IV. Formulation 1, which is currently being tested, is considered as the baseline hydroxy-terminated polybutadiene formulation for the initial test series. Formulations 2, 3, and 4 are selected for investigation of the inter-related effects of oxidizer particle size and base (no crossflow) burning rate. Formulations 1 and 4 are essentially identical, except for use of burning rate catalyst to change base burning rate. Formulations 2 and 3 differ from Formulation 1 in oxidizer particle size, and as a consequence, also in base burning rate. Comparison of results from tests with these four formulations should permit isolation of the oxidizer particle size and base burning rate effects on sensitivity of propellant burning rate to crossflow. Formulation 5 differs from Formulation 1 mainly with respect to mixture ratio (which also affects flame temperature and base burning rate): comparison of erosion sensitivities of these formulations will be used to study the effect of mixture ratio. Formulation 6 has been chosen as a baseline polyester propellant for comparison with the HTPB formulations, to see whether binder type has a significant effect on erosion sensitivity, and also to serve for comparison with further polyester formulations. Strand burning rate data for Formulations 1 through 4 are presented in Figure 7, while predicted erosive burning characteristics for Formulation 1 (calculated using the strand data and the previously described computer code) are given in Figure 8.

Parametric design studies involving development of interior ballistics computer codes for the test apparatus have been employed for definitition of specific tests to be run with formulations 1 through 4. In this process, several possible initial operating pressures are first chosen for nozzleless tests and for tests with various possible nozzle sizes. Simplified ballistic equations, neglecting cross-velocity effects and axial pressure variations in the test section, are then used to calculate the required driver grain lengths, total propellant weights, burn times, and final operating pressures for these chosen initial pressure and nozzle (or no nozzle) configurations. The

calculated driver grain lengths and nozzle configurations are then input, along with the propellant characteristics, to detailed interior ballistics computer codes derived for the test apparatus configuration (separate codes for the nozzled and nozzleless cases), which allow for dependency of burning rate on crossflow velocity (assumed sensitivities are investigated parametrically), and also allow for compressibility effects including total pressure losses associated with mass addition to a flowing stream, for calculation of static pressure and crossflow velocity versus time and axial location. These results are then examined and a test matrix which will cover a desired range of pressure and cross flow velocity for a given formulation is selected. A matrix of 25 tests selected for study of Formulations 1 through 4 is presented in Table V.

Tests 1 through 6 comprise the basic test matrix for Formulation 1. In Figure 9, the pressure-crossflow velocity domain covered by Tests 1 through 3 is plotted. As may be seen, these tests permit obtaining of burning rate at 3 pressures at any value of crossflow velocity from about 150 to 400 m/sec (500 to 1300 ft/sec): it is believed that this amount of data is adequate for characterization of erosive burning effects over this crossflow velocity range. Additional tests, of course, can be run to obtain more pressures at each crossflow velocity at a cost of one test per additional pressure value, if desired. In Figure 10, predicted static pressure versus time traces at the aft window of the test section are presented for Tests 4 through 6. As indicated on the curves, the crossflow velocities are essentially constant at 850 m/sec (2800 ft/sec) during these tests, while during the course of the three tests the entire pressure range from 580,000 to 5,100,000 N/m^2 (85 to 740 psia) is covered, permitting thorough evaluation of burning rate versus pressure at 850 m/sec (2800 ft/sec). Similar plots for the other three windows in the test section indicate the same sort of pressure range coverage for crossflow velocities of 730 m/sec (2400 ft/sec), 670 m/sec (2200 ft/sec), and 610 m/sec (2000 ft/sec), though the crossflow velocity varies slightly from test to test at the farthest upstream location, requiring some crossplot corrections to a common velocity. Thus, it appears that six tests may be used to fairly thoroughly characterize the erosive burning of the baseline formulation at crossflow velocities of 150 to 400, 610, 670, 730, and 850 m/sec (500 to 1300, 2000, 2200, 2400, and 2800 ft/sec) over an appreciable pressure range.

Tests 7 and 8 are aimed at establishing how sensitive the erosive burning behavior of the test propellant is to the initial boundary layer characteristics. Basically, these tests are repeats of Tests 1 and 3, with the section of rectangular grain in the tranisition section removed. Thus, instead of a boundary layer flow which has had a chance to develop from back at the leading edge of the driver grain, we have a sharp leading edge corner at the beginning of the test grain, a markedly different starting condition.

Tests 9 and 10 will also be compared directly with Tests 1 and 3, this time for study of the effect of driver grain flame temperature on erosive burning of a given propellant. (Recall that Marklund and Lake found the effect of varying driver grain temperature to be negligible. This is a very important point as regards the basic assumption of the Lenoir and Robillard and related core-gas heat transfer models as pointed out earlier, and should be tested further.)

Tests 11 through 15 will repeat 5 of the 6 test conditions employed in characterizing the baseline propellant for Formulations 2, 3, and 4, providing information regarding the dependency of erosive burning of composite propellants on ammonium perchlorate particle size and base (no crossflow) burning rate.

Preliminary Test Results

To date, two successful tests have been carried out with Formulation 1 in the hardware described above. As indicated in Table I, Formulation 1 is a 73 percent AP, 27 percent HTPB binder (including 0.05 percent carbon black as an opacifier) formulation with unimodel 20μ oxidizer. Preliminary results of these tests are presented and compared with predictions (made using the model described earlier) in Figure 11, where the burning rate augmentation ratio is plotted against crossflow velocity. Approximately the same range of crossflow velocities was covered in each test, the major difference between the tests being the pressure levels. (These tests are numbers 1 and 3 in the test matrix presented in Table V.) As may be seen, the general level of burning rate augmentation observed agrees reasonably well with the predictions, with the higher pressure level resulting in higher augmentation ratios, as predicted. The observed dependence of burning rate augmentation on crossflow velocity, however, does appear to be stronger than predicted at low pressure. It must be emphasized that these results are quite preliminary. The method of inhibiting the sides of the regressing surface of the test propellant has not yet been optimized, with the result that the inhibitor does not regress cleanly with the propellant, resulting in some difficulty in determination of instantaneous burning rates from the movie films. In addition, the optics and film scaling methods have not yet been perfected to give the maximum yield (in quantity and quality) of instantaneous burning rate data. As the test program progresses, these problems will be resolved, and better quality data will be obtained. At this point, the experimental equipment appears quite promising as a tool for erosive burning characterization of a propellant.

SUMMARY

Past modeling efforts in the area of erosive burning of solid propellants have been reviewed and lack of a model which incorporates a realistic description of composite propellant combustion has been noted. A possible physical mechanism by which crossflows may affect the combustion of a composite propellant has been postulated and a mathematical model for prediction of the burning rate of a composite propellant in such a crossflow, given only the no-crossflow burning rate versus pressure characteristics of the propellant, has been developed. This model has been used to predict remarkably well the erosive burning characteristics of a propellant studied by Saderholm (2). In addition, a test device for studying the erosive burning characteristics of a propellant in high velocity crossflows (up to Mach 1) has been constructed and testing begun. Preliminary test results have been obtained and are in fair agreement with predictions made using the aforementioned model.

REFERENCES

1. Viles, J.M, "Prediction of Rocket-Motor Chamber Pressures using Measured Errosive-Burning Rates," Technical Report S-275 (Contract DAAHO1-70-C-

0152) Rohm and Haas Co., Huntsville, Alabama 35807, October, 1970. CONFIDENTIAL.

2. Saderholm, C. A., "A Characterization of Erosive Burning for Composite H-Series Propellants," AIAA Solid Propellant Rocket Conference, Palo Alto, California, January 29, 1964.

3. Kreidler, J. W., "Erosive Burning: New Experimental Techniques and Methods of Analysis," AIAA Solid Propellant Rocket Conference, Palo Alto, California, January 29, 1964.

4. Schultz, R., Green, L., and Penner, S. S., "Studies of the Decomposition Mechanism, Erosive Burning, Sonance and Resonance for Solid Composite Propellants," Combustion and Propulsion, 3rd AGARD Colloquium, Pergamon Press, N. W., 1958.

5. Green, L., "Erosive Burning of Some Composite Solid Propellants," Jet Propulsion, 24, 9, 1954.

6. Peretz, A., "Experimental Investigation of the Erosive Burning of Solid Propellant Grains with Variable Port Area," AIAA Journal, 6, 910, 1968.

7. Marklund, T., and Lake, A., "Experimental Investigation of Propellant Erosion, ARS Journal, 30, 173, 1960.

8. Dickinson, L. A., Jackson, F., and Odgers, A. L., "Erosive Burning of Polyurethane Propellants in Rocket Engines," Eighth Symposium (International on Combustion, 754, Williams and Wilkins, Baltimore, 1962.

9. Zucrow, M. J., Osborn, J. R., and Murphy, J. M., "An Experimental Investigation of the Erosive Burning Characteristics of a Nonhomogeneous Solid Propellant," AIAA Journal, 3, 523, 1965.

10. Vilyunov, V. N., Dvoryashin, A. A., Margolin, A. D., Ordzhonikidze, S. K., and Pokhil, P. F., "Burning of Ballistite Type H in Sonic Flow," Fizika Goreniya i Vzryva, 8, 4, 501-5, October - December, 1972.

11. Lenoir, J. M., and Robillard, G., "A Mathematical Method to Predict the Effects of Erosive Burning in Solid-Propellant Rockets," Sixth Symposium (International) on Combustion, 663, Reinhold Publishing Corp., New York, 1957.

12. Zucrow, M. J., Osborne, J. R., and Murphy, J. M., "The Erosive Burning of a Nonhomogeneous Solid Propellant, "AICHE Symposium Series No. 52, 23-29, 1964.

13. Corner, J., Theory of the Interior Ballistics of Guns, John Wiley and Sons, Inc., New York, 1950.

14. Zeldovich, Y. B., "Theory of Propellant Combustion in a Gas Flow," Fizika Goreniya i Vzryva, 7, 4, 463-76, October - December, 1971.

15. Vilyunov, V. N., et al., "Burning of Ballistite Type H in Sonic Flow," Fizika Goreniya i Vzryava, 8, 4, 501 - 505, October - December, 1972.

16. Vanderkerchove, J., "Erosive Burning of a Colloidal Solid Propellant," Jet Propulsion, 28, 599, 1958.

17. Lengelle, G., "Model Describing the Erosive Combustion and Velocity Response of Composite Propellants," AIAA Journal. 13, 3, 315-322, March, 1975.

18. Sanderholm, C. A., Biddle, R. A., Caveny, L. H., and Summerfield, M., "Combustion Mechanisms of Fuel Rich Propellants in Flow Fields," AIAA Paper No. 72-1145, presented at AIAA/SEA 8th Joint Propulsion Specialist Conference, New Orleans, Louisiana, November 29, 1972.

19. Tsuji, H., "An Aerothermochemical Analysis of Erosive Burning of Solid Propellant," Ninth International Symposium on Combustion, 384-393, 1963.

20. Geckler, R. E., et al., Aerojet Engineeirng Corporation Report 445, 1950.

21. King, M., "A Modification of the Composite Propellant Erosive Burning Model of Lenoir and Robillard," Combustion and Flame, 24, 365-368, 1975.

22. Williams, F. A., Barrere, M., and Huang, N. C., "Fundamental Aspects of Solid Rockets, AGARDograph No. 116, Chapter 7, 396-456, NATO, October, 1969.

23. Mickley, H. S., and Davis, R. S., "Momentum Transfer for Flow Over a Flat Plate with Blowing," NACA Technical Note 4017, November, 1957.

24. Sutherland, G. S., "The Mechanism of Combustion of an Ammonium Perchlorate-Polyester Resin Composite Solid Propellant," Ph.D. Thesis, Princeton, 1956.

Table I. General Types of Models of Erosive Burning Developed to Date.

1. MODELS BASED ON HEAT TRANSFER FROM A "CORE GAS" IN THE PRESENCE OF CROSS FLOW

   e.g LENOIR & ROBILLARD (11)
   ZUCROW, OSBORNE AND MURPHY (12)
   SADERHOLM (2)
   MARKLUND (7)

2. MODELS BASED ON ALTERATION OF TRANSPORT PROPERTIES IN REGION FROM SURFACE TO FLAME ZONE BY CROSSFLOW, GENERALLY DUE TO TURBULENCE EFFECTS. INCLUDES EFFECTS ON CONDUCTIVITY FROM FLAME ZONE BACK TO PROPELLANT AND EFFECTS ON TIME FOR CONSUMPTION OF FUEL POCKETS LEAVING SURFACE.

   e.g SADERHOLM, BIDDLE, CAVENY, et al (18)
   LENGELLÉ (17)
   CORNER (DOUBLE-BASE) (13)
   VANDERKERCHOVE (DOUBLE-BASE) (16)
   ZELDOVICH (DOUBLE-BASE) (14)
   VILYUNOV (DOUBLE-BASE) (15)
   GECKLER (20)

3. MODELS BASED ON CHEMICALLY REACTING BL THEORY (HOMOGENEOUS SYSTEMS ONLY)

   e.g TSUJI (19)

Table II. Summary Review of Current Most Commonly Used Erosive Burning Model, That of Lenoir and Robillard (11).

$$r = a P^n + \alpha G^{0.8} L^{-0.2} \exp(-\beta \dot{m}/G)$$

BASIS: ADDITION OF CONVECTIVE HEAT TRANSFER FROM THE CROSS-FLOW MAINSTREAM TO THE PROPELLANT SURFACE TO THE HEAT FEEDBACK PROVIDED BY THE PROPELLANT FLAME ZONES.

SHORTCOMINGS:

(1) DOES NOT ACCOUNT FOR THE EFFECTS OF THE CROSS-FLOW ON THE DETAILS OF THE GAS-PHASE MIXING AND REACTION PROCESSES

(2) THE ADDITIVITY OF THE HEAT FLUXES FROM THE MAINSTREAM AND THE PROPELLANT FLAME ZONES IS HANDLED INCORRECTLY

(3) THE MODEL CONTAINS TWO FREE CONSTANTS (IN ADDITION TO THOSE ASSOCIATED WITH THE NONEROSIVE BURNING BEHAVIOR) WHICH MUST BE OBTAINED BY DATA FITTING FOR EACH PROPELLANT

(4) THE MODEL PREDICTS SUBSTANTIAL DEPENDENCE OF BURNING RATE ON THE MAINSTREAM GAS TEMPERATURE; SUCH DEPENDENCE WAS FOUND BY MARKLUND AND LAKE TO BE COMPLETELY ABSENT

Table III. Calculation of Cross-flow Velocity Profile in Current Erosive Burning Model.

1. NEGLECTING TRANSPIRATION EFFECTS

$$\text{CALCULATE} \quad U^* = U_{\text{Mainstream}} \sqrt{\frac{f}{2}} = \frac{0.152\, U_{\text{Mainstream}}}{(\text{Re})^{0.1}}$$

$$= \frac{0.023\, (U_{\text{Mainstream}}^{0.9})\, (273 + T_{\text{Flame}})^{0.18}}{D^{0.1}\, \rho^{0.1}}$$

$$\text{CALCULATE} \quad Y^+ = Y U^* \rho / u$$

$$\text{CALCULATE} \quad U^+ = Y^+ \text{ FOR } Y^+ < 5$$

$$U^+ = -3.05 + 5.00 \text{ LN } Y^+ \text{ FOR } 5 < Y^+ < 30$$

$$U^+ = 5.5 + 2.5 \text{ LN } Y^+ \text{ FOR } Y^+ > 30$$

$$\text{CALCULATE} \quad U = U^+ U^*$$

2. ALLOWING FOR TRANSPIRATION (USING DATA OF MICKLEY AND DAVIS) DO ALL OF THE ABOVE AND CORRECT RESULT BY

$$U_{\text{Transpiration Case}} = U_{\text{No Transpiration}}\, \exp\left(-60\, U_{\text{Gas, Transpiration}}/U_{\text{Main}}\right)$$

Table IV. Formulations Selected For Initial Characterization in the Erosive Burning Test Apparatus.

FORMULATION NUMBER	COMPOSITION (WT %)	FLAME TEMP. (°K)	DENSITY gm/cc (lb/in^3)	PRODUCT MOLECULAR WEIGHT	SPECIFIC HEAT RATIO	C* m/sec (ft/sec)	RATIONALE FOR SELECTION
1	73 AP/27 HTPB 20 MICRON AP	1667	1.49 (.0539)	19.2	1.30	1275 (4182)	BASELINE UNIMODAL AP HTPB FORMULATION
2	73 AP/27 HTPB 200 MICRON AP	1667	1.49 (.0539)	19.2	1.30	1275 (4182)	COMPARISON WITH #1 FOR AP SIZE EFFECT
3	73 AP/27 HTPB 3 MICRON AP	1667	1.49 (.0539)	19.2	1.30	1275 (4182)	COMPARISON WITH #1, #2 FOR AP SIZE EFFECT
4	72 AP/26 HTPB/ 2 Fe_2O_3 20 MICRON AP	1642	1.52 (.0550)	20.1	1.30	1266 (4150)	COMPARISON WITH #1 FOR BR EFFECT AT CONSTANT AP SIZE
5	77 AP/23 HTPB 20 MICRON AP	2065	1.55 (.0559)	20.7	1.30	1375 (4510)	COMPARISON WITH #1 FOR MIX RATIO (TEMPERATURE) EFFECT AT CONSTANT AP SIZE
6	65 AP/35 POLY-ESTER 20 MICRON AP	1850	1.60 (.0577)	22.0	1.26	1269 (4162)	BASELINE POLYESTER FORMULATION COMPARE WITH #1 FOR BINDER EFFECT.

Table V. Test Matrix For Formulations 1 — 4.

Test No.	Formulation	Nozzle Gap (cm)	Nozzle Gap (inches)	Initial Total Pressure $(n/m^2)\times10^{-6}$	Initial Total Pressure (psia)	Driver Length (cm)	Driver Length (inches)	Final Total Pressure $(n/m^2)\times10^{-6}$	Final Total Pressure (psia)
1	1	1.27	0.5	1.378	200	11.2	4.4	2.618	380
2	1	1.27	0.5	2.412	350	16.0	6.3	4.685	680
3	1	1.27	0.5	4.134	600	22.4	8.8	8.200	1190
4	1	N	N	2.067	300	22.9	9.0	0.861	125
5	1	N	N	4.134	600	34.8	13.7	1.791	260
6	1	N	N	8.268	1200	51.8	20.4	3.583	520
7	1	1.27	0.5	1.378	200	11.2	4.4	2.618	380
8	1	1.27	0.5	4.134	600	22.4	8.8	8.200	1190
9	1	1.27	0.5	1.378	200	8.6	3.4	2.480	360
10	1	1.27	0.5	4.134	600	18.0	7.1	8.000	1160
11	2	1.27	0.5	1.378	200	20.6	8.1	2.894	420
12	2	1.27	0.5	2.412	350	27.9	11.0	5.133	745
13	2	1.27	0.5	4.134	600	37.3	14.7	8.888	1290
14	2	N	N	2.067	300	39.9	15.7	0.827	120
15	2	N	N	4.134	600	57.4	22.6	1.585	230
16	3	1.27	0.5	1.378	200	8.1	3.2	3.445	500
17	3	1.27	0.5	2.412	350	10.4	4.1	6.339	920
18	3	1.27	0.5	4.134	600	13.0	5.1	10.950	1590
19	3	N	N	4.134	600	20.3	8.0	0.930	135
20	3	N	N	8.268	1200	26.4	10.4	1.894	275
21	4	1.27	0.5	1.378	200	4.6	1.8	2.205	320
22	4	1.27	0.5	2.412	350	7.1	2.8	4.065	590
23	4	1.27	0.5	4.134	600	10.9	4.3	7.372	1070
24	4	N	N	4.134	600	17.5	6.9	1.860	270
25	4	N	N	8.268	1200	27.7	10.9	3.790	550

[a]N= Nozzleless

[b]No grain in transition section

[c]2400 °K Driver Propellant To Test Driver Temperature Effect - Matched Ballistics

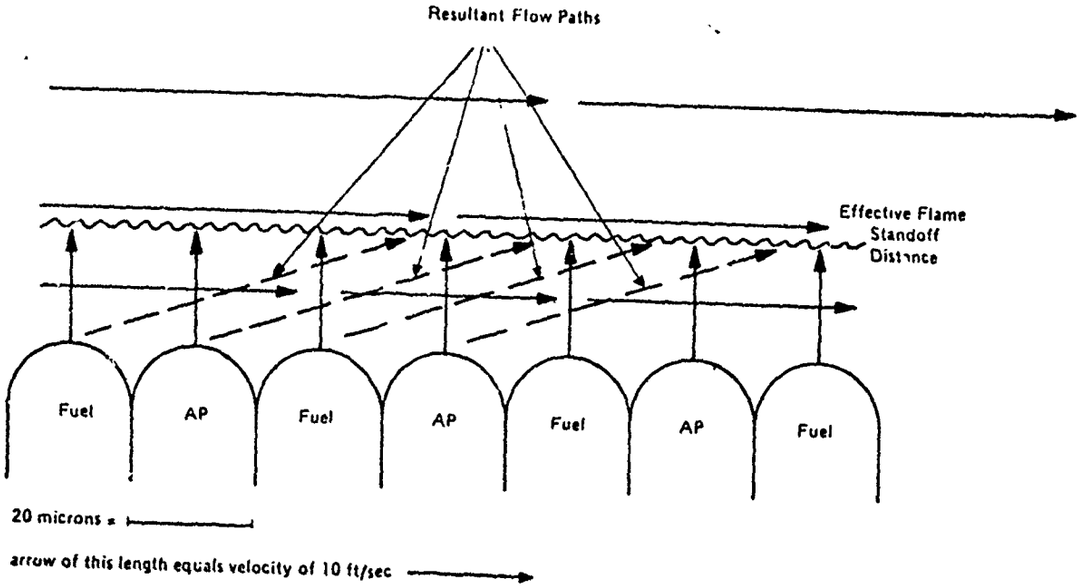

Figure 1. Diagrammatic Representation of Scales of Processes in Composite Propellant Burning at 0.5 in/sec at 1000 psia in a Crossflow of 300 ft/sec with 20 micron degree of Heterogeneity.

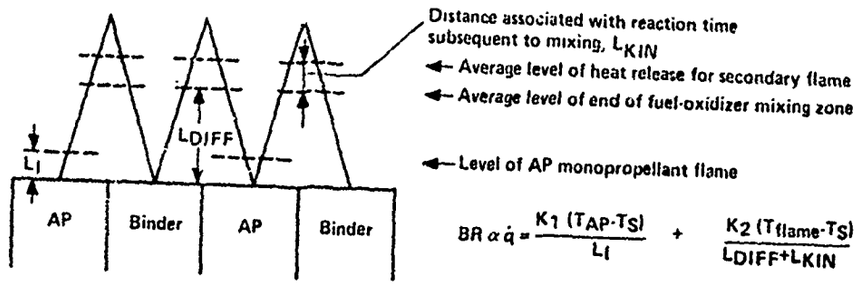

a) No cross-flow velocity

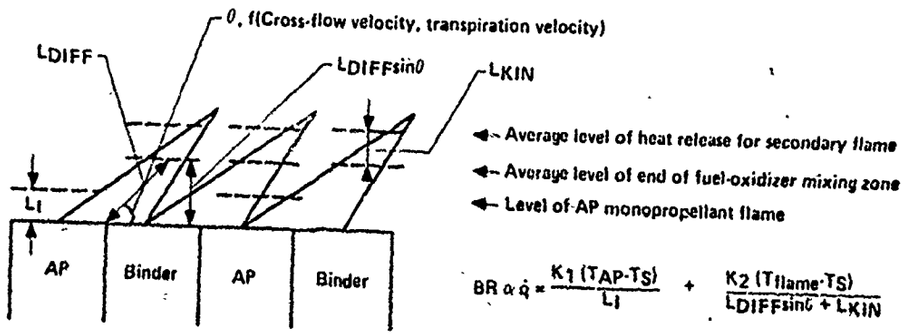

b) Cross-flow, L_{KIN}, L_{DIFF}, L_l = f($\dot{m}_{burn}$, P) alone, independent of cross-flow angle

Figure 2. Schematic of Geometrical Model of Erosive Burning (Two-Flame Model).

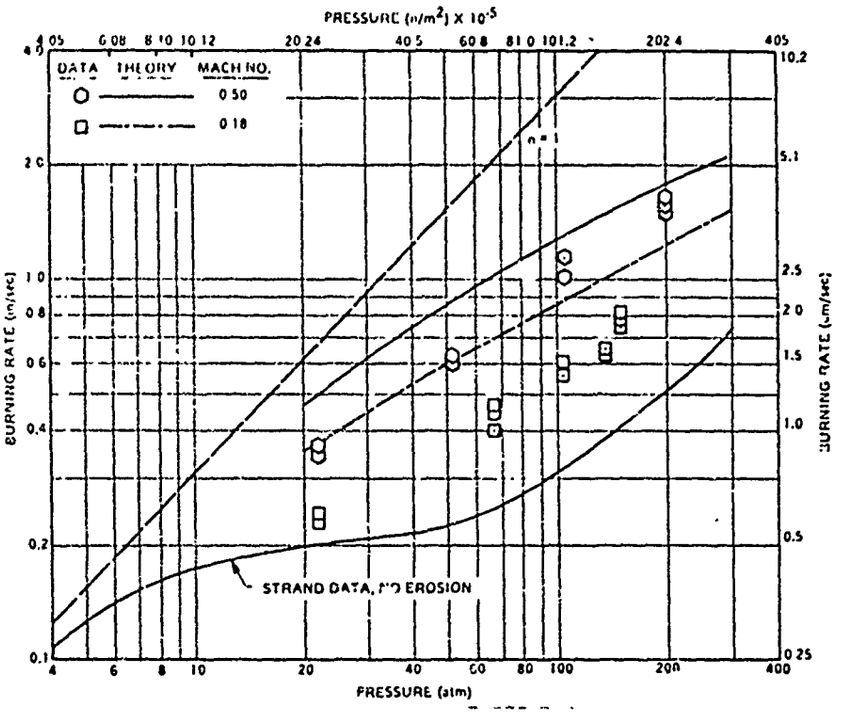

Figure 3. Erosive Burning Model Predictions and Comparisons with Saderholm Data. Transpiration Effects not Included.

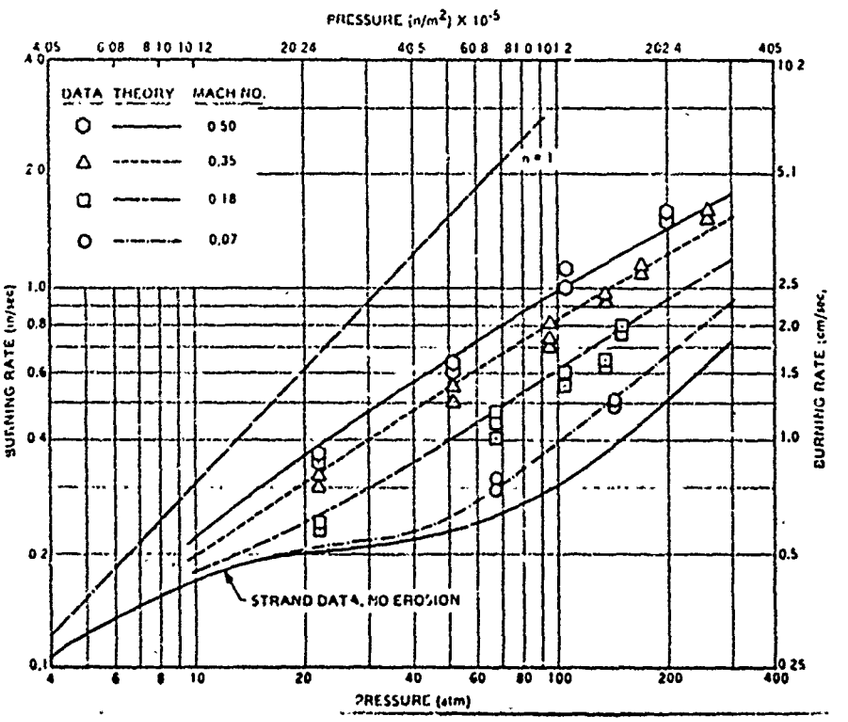

Figure 4. Erosive Burning Model Predictions and Comparisons with Saderholm Data. Transpiration Effects Included.

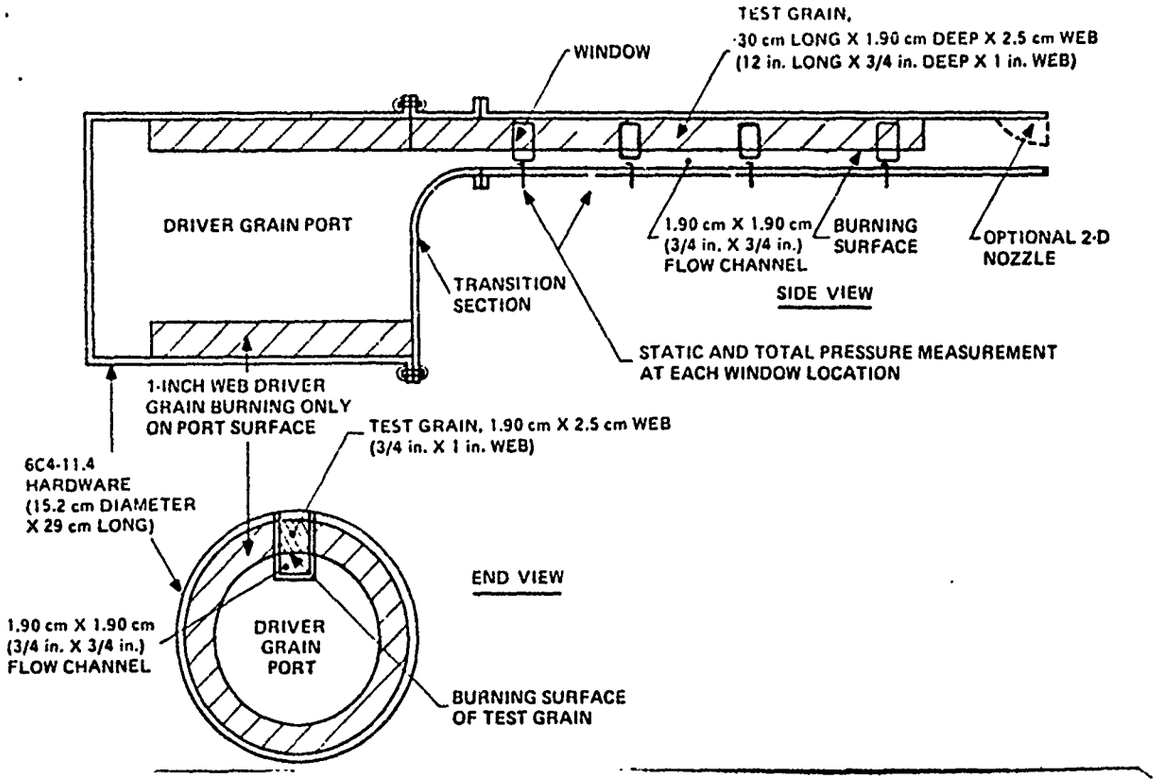

Figure 5. Sketch of Test Hardware.

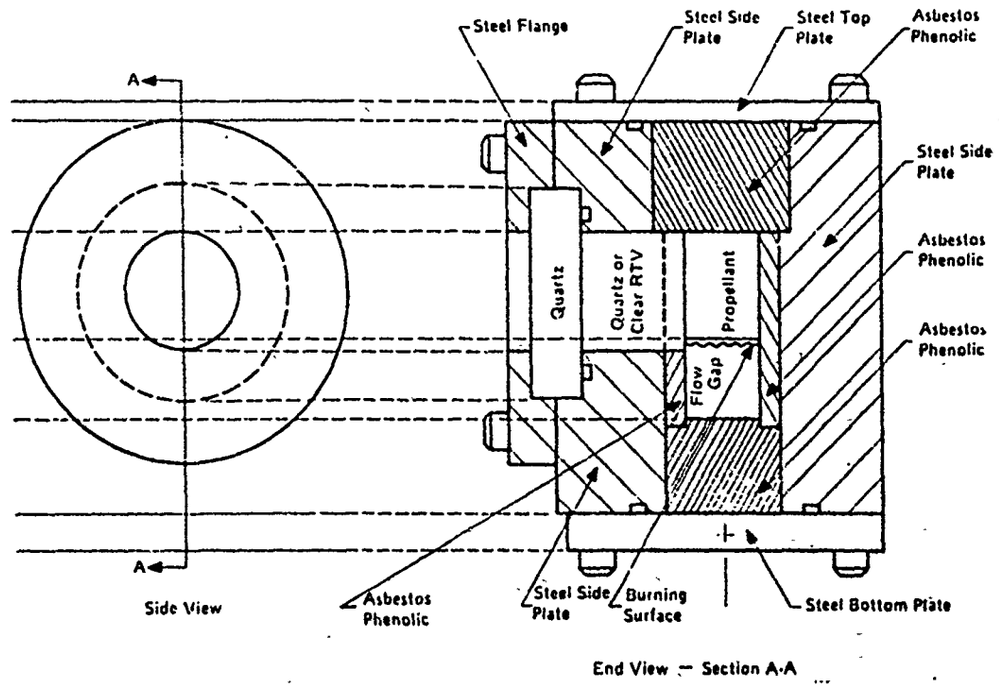

Figure 6. Test Section Detail, Emphasizing Viewing Windows.

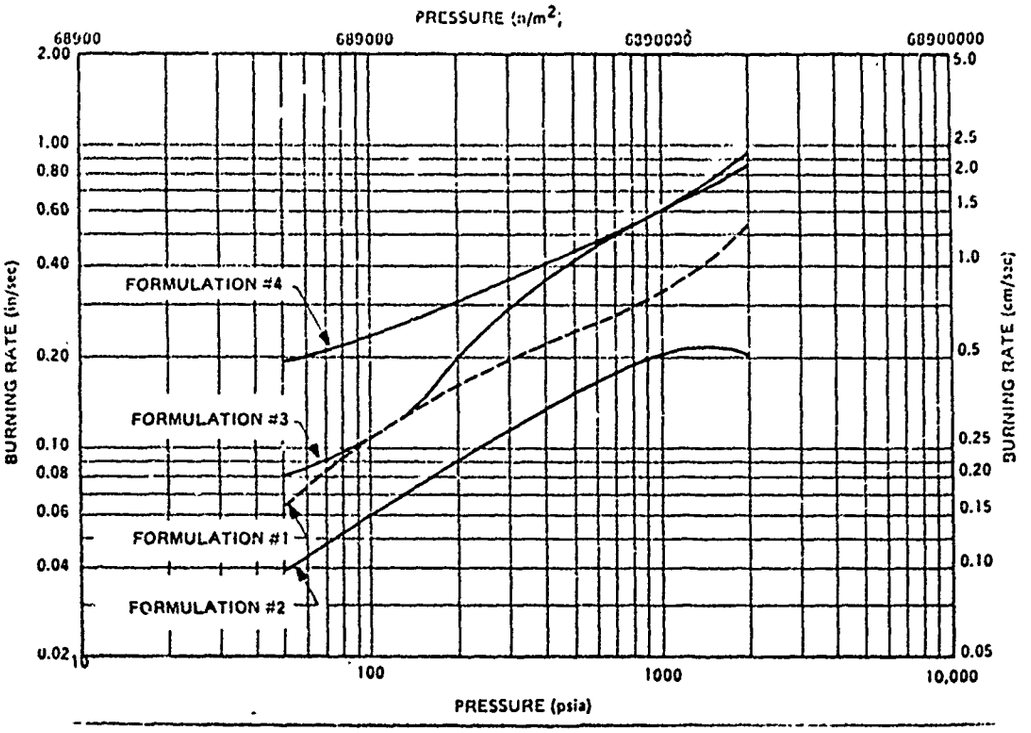

Figure 7. Strand Rate Burning Data For First Four Test Formulations.

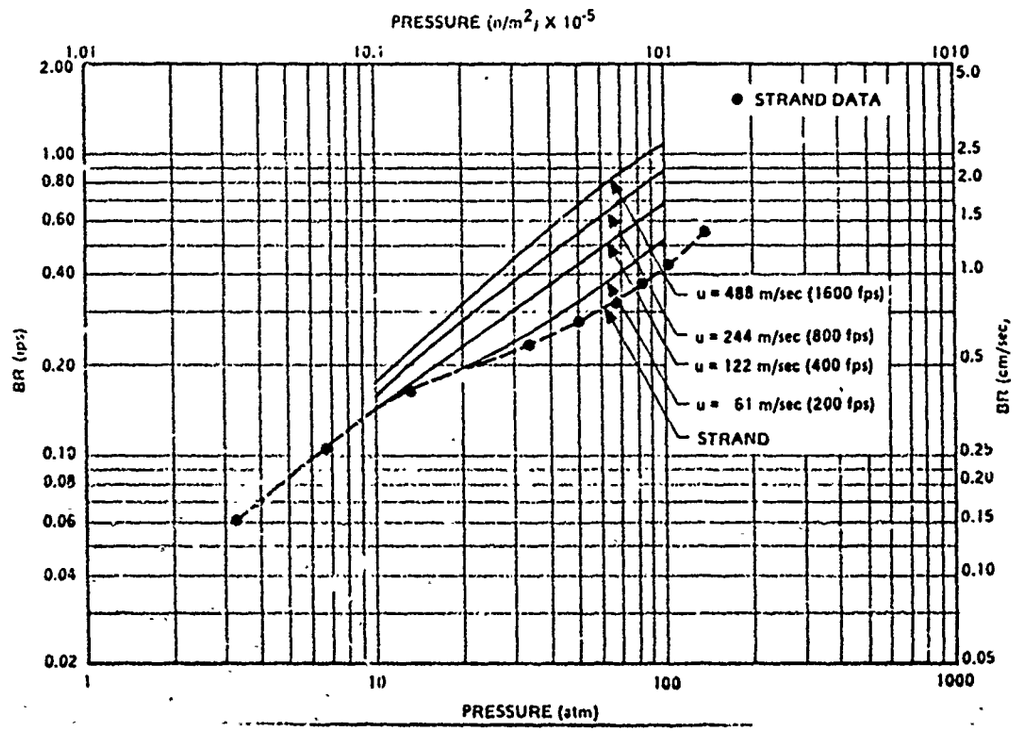

Figure 8. Predicted Erosive Burning Characteristics of Test Formulation Number 1.

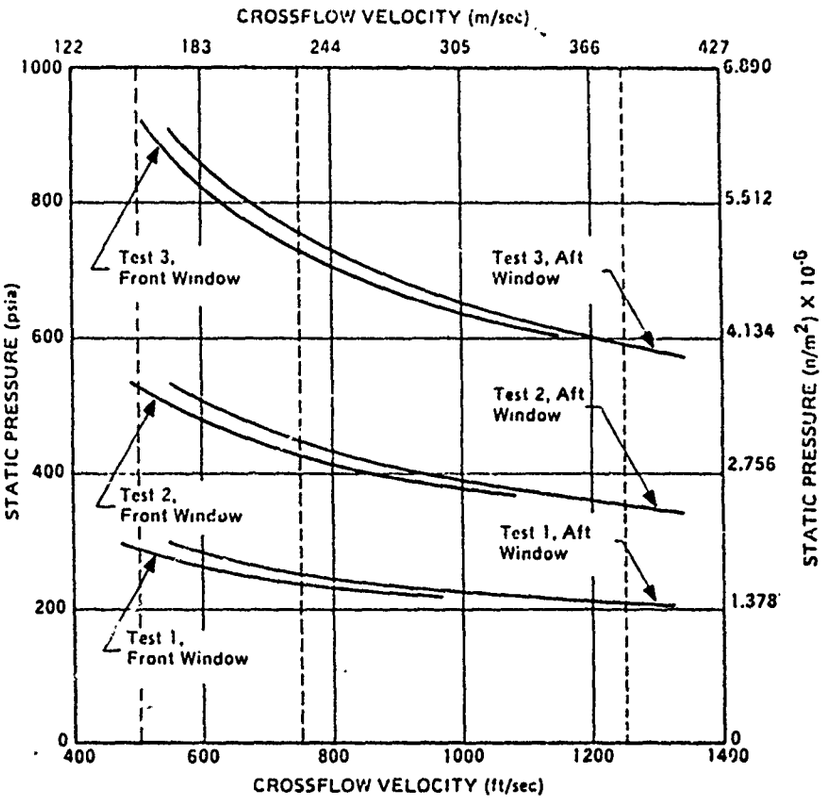

Figure 9. Pressure - Crossflow Velocity Domain Covered by Tests 1, 2 and 3.

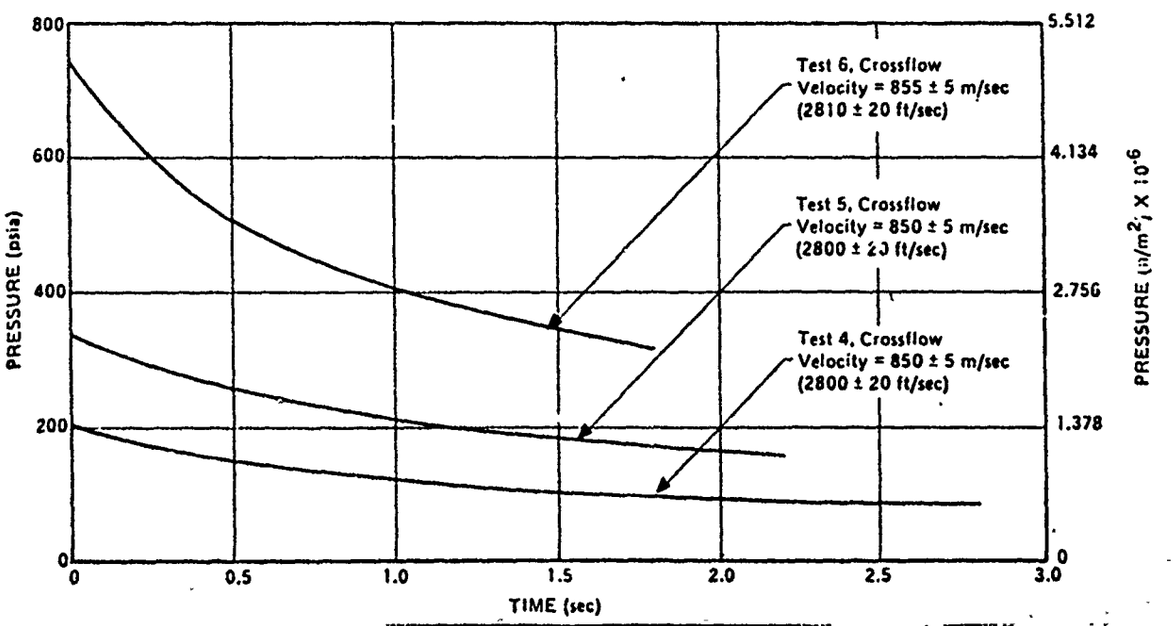

Figure 10. Pressure Versus Time at Aft Window - Predictions For Tests 4,5,6.

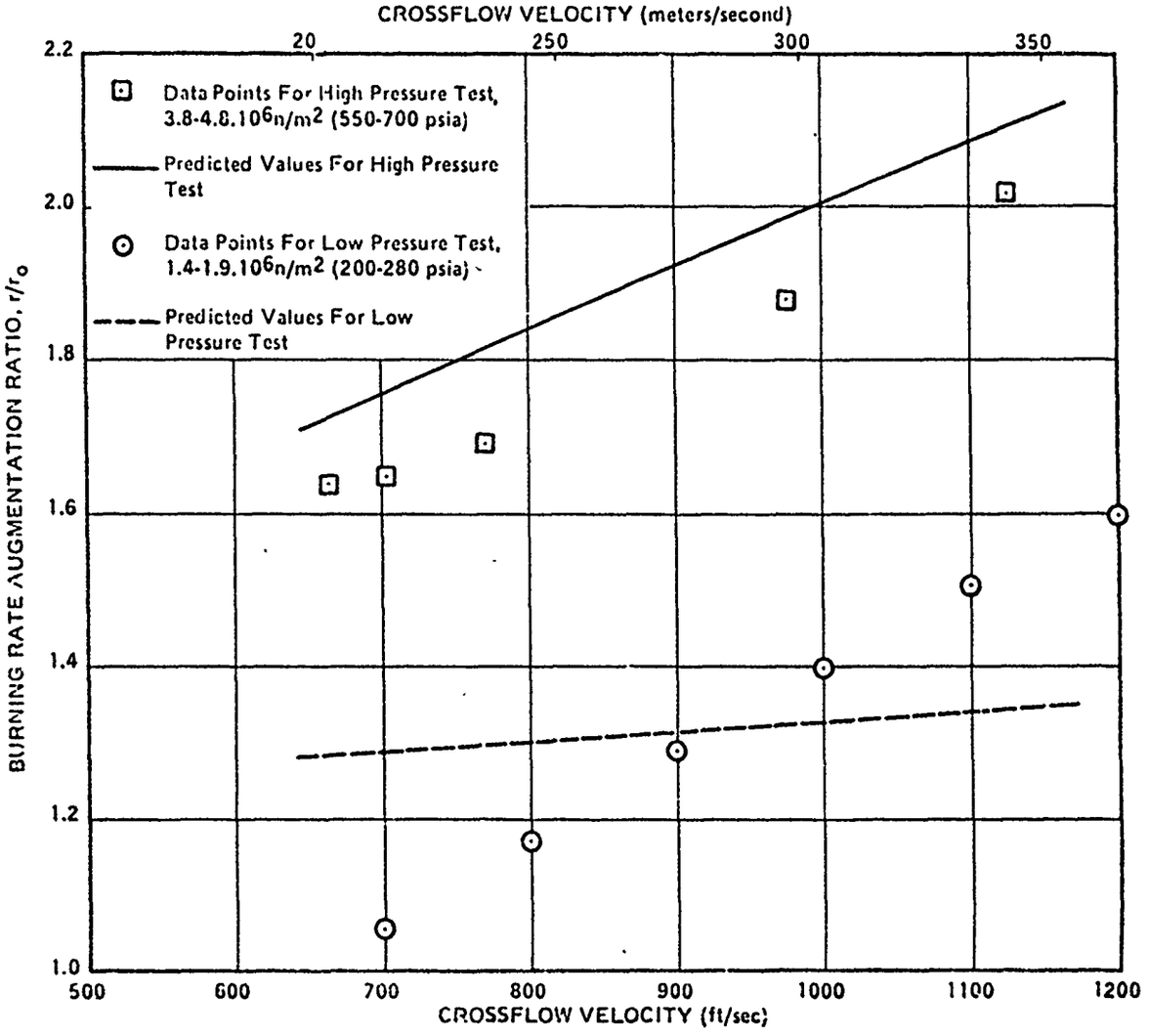

Figure 11. Preliminary Results of Two Tests with Formulation #1 at Low and High Pressure